Journal of Volcanology and Geothermal Research 421 (2022) 107421

Contents lists available at ScienceDirect

Journal of Volcanology and Geothermal Research

journal homepage: www.elsevier.com/locate/jvolgeores

Wavelet-based filtering and prediction of soil CO_2 flux: Example from Etna volcano (Italy)

Salvatore Scudero [a,*], Antonino D'Alessandro [a], Giovanni Giuffrida [b], Sergio Gurrieri [b], Marco Liuzzo [b]

[a] Istituto Nazionale di Geofisica E Vulcanologia, Osservatorio Nazionale Terremoti, Rome, Italy
[b] Istituto Nazionale di Geofisica E Vulcanologia, Sezione di Palermo, Palermo, Italy

ARTICLE INFO

Article history:
Received 6 August 2021
Received in revised form 21 October 2021
Accepted 24 October 2021
Available online 30 October 2021

Keywords:
Soil CO_2
Continuous wavelet transform
Spectral analysis
Etna

ABSTRACT

In this work, we propose a wavelet-based filtering for soil CO_2 flux time series. The filter relies on the detection of the periodic components achieved by means of the long-term time-frequency characterization of the time series. For this purpose, we exploited the vast data set coming from the monitoring network installed at Mt. Etna volcano (Italy). The network provides hourly measure of CO_2 flux together with the measure of the climatic variables. These data allow to investigate the relationships between CO_2 time series and the potentially influencing meteorological factors. This has been assessed calculating the wavelet coherence between CO_2 time series against air temperatures, atmospheric pressure, and relative humidity in all the sites where these information were available. Results highlight the occurrence of marked cycles at about ~1 year for the most of the sites while shorter cycles occur only at some sites. From these cycles a periodic signal can be calculated, and therefore opportunely removed from the time CO_2 series to enhance the volcano-related anomalies. We found also common cycles among CO_2 and the climatic variables, which synchronicity is constant over time but it is site-specific. Starting from this consideration, we calculated a reference signal for CO_2 combining analytically the temperature, the pressure, and the humidity cycles: this model of the climatic effect has been used to predict the seasonal trend of the CO_2 output.

1. Introduction

Monitoring of diffuse soil CO_2 has become very important in recent years and allows to better understand the variations of volcanic activity in terms of recognizing episodes of volcanic unrest and precursors of eruptive periods as well. The development and implementation of permanent automatic CO_2 flux stations has made it possible to obtain long time series of data in different volcanic contexts.

The dynamics of soil CO_2 is quite complex and depends on many different factors acting simultaneously. One over all is given by the climatic-environmental variables which influence the CO_2 output resulting in a series of marked periodic variations of the signal. Other environmental (e.g. weather episodes), geological (e.g. changes in ground permeability or in the circulation of geofluids), or seismo-volcanic (e.g. earthquake occurrence, magma ascent, unrest) processes may result in non-periodic (high frequency-anomalies, trend, long-range memory, etc.) effects. The environmental meteorological phenomena may account for up to 50% of the fluxes values measured (Granieri et al., 2003, 2010; Viveiros et al., 2009, 2015), therefore the problem of their removal has raised. To achieve this, statistical filtering techniques have been used in order to separate the magmatic component from external influences. The methodologies proposed for filtering are various and include, among the most widely adopted: Fourier transform based filters, multiple linear regressions, and moving-average filters (Granieri et al., 2003; Liuzzo et al., 2013; Oliveira et al., 2018). In recent years the application of the wavelet methodology expanded to many fields of interest and, among the possible applications, it has been successfully employed for the study of various geochemical time series. This technique is sometimes preferred to the Fourier analysis, because of its capability to easier identify sparse portions of regular signals, transients, or singularities (Mallat, 1999).

The recent literature provides several examples of the application of the wavelet analysis for the study of various geochemical time series and in particular, as a method for the detection of short- and long-term periodicity in soil gas signals, both in volcanic and non-volcanic settings (Lewicki and Hilley, 2014; Lewicki et al., 2017; Yan et al., 2017; Oliveira et al., 2018; Oh et al., 2019; Siino et al., 2019, 2020; D'Alessandro et al., 2020), and also in volcanic plume emissions (Boichu et al., 2010; Tamburello et al., 2013; Pering et al., 2014, 2019; Ilanko et al., 2015). The availability of numerous and long-lasting soil

* Corresponding author.
E-mail address: salvatore.scudero@ingv.it (S. Scudero).

https://doi.org/10.1016/j.jvolgeores.2021.107421

CO_2 time series from a monitoring network operating at Mt. Etna volcano (Italy) allowed us to test the application of the wavelet technique for their spectral analysis in the time-frequency domain.

In particular, the CO_2 flux time series from Mt. Etna represent a unique data set because of the continuity of observations and also because of the availability of the climatic information recorded at the same sites (air temperature, atmospheric pressure, and relative humidity). The reason of such complete set of data at Mt. Etna relies on the importance of CO_2 flux to get insights into various eruptive processes (Liuzzo et al., 2013; Cannata and Coauthors, 2015; Gurrieri et al., 2021).

In this paper, we perform a power spectral analysis in the time-frequency domain by means of continuous wavelet transformation to investigate the soil CO_2 time series and the coherency, in pairs, with climatic variables. The adopted methodology proves to be useful for filtering and prediction purposes. The filtered signals of soil CO_2 flux will allow volcanologists to explore in depth the relationships between soil gas emissions and volcanic processes.

2. Method and data

The time series have been analysed in the frequency domain by means of the Continuous Wavelet Transform (CWT). This technique includes some advantages with respect to other methods, in particular its flexibility which allows the detailed analysis of the temporal continuity of the periodic components within irregular, non stationary, non periodic signals (Sifuzzaman et al., 2009). In this paragraph, we introduce the basic theory of the continuous wavelet transformation on the basis of the notations reported by Daubechies (1992) and Conraria and Soares (2011).

We also present the field data: how they have been collected and their general statistical characterization.

2.1. Wavelet analysis

In general terms, a Wavelet Transform (WT) is the decomposition of a signal into a set of basic functions consisting of contractions, expansions, and translations of a function $\psi(t)$, called the mother wavelet (Daubechies, 1992). Let consider the space $L^2(R)$ as the set of square integrable functions which satisfy $\int_{-\infty}^{+\infty}|g(t)|^2\mathrm{d}t<\infty$, and with the capital letter, G(t) the Fourier transformation of a given function, $G(\omega)=\int_{-\infty}^{+\infty}g(t)e^{(-i\omega t)}\mathrm{d}t$. A function $\psi(t)\in L^2(R)$ which satisfies the condition of admissibility $\Psi(0)=\int_{-\infty}^{+\infty}\psi(t)\mathrm{d}t=0$ is called "mother wavelet", and a double-indexed family ("wavelet daughters") is introduced by translating and scaling $\psi(\cdot)$: $\psi_{\tau,s}(t)=|s|^{-1/2}\psi\left(\frac{t-\tau}{s}\right)$ with s, $\tau\in R$ and $s\neq 0$.

For the application of this paper, we adopted the well-known, quite flexible, and complex-valued Morlet mother wavelet which has the following form: $\psi(t)=\pi^{-1/4}e^{i\omega t}e^{-t^2/2}$. The local Wavelet Power Spectrum (WPS) based on the CWT of a given function $g(t)\in L^2(R)$ with respect to the wavelet family is:

$$|\mathrm{WPS}|_g(\tau,s)=|W_{x;\psi}(\tau,s)|^2=\left|\int_{-\infty}^{+\infty}g(t)|s|^{-1/2}\psi^*\left(\frac{t-\tau}{s}\right)\mathrm{d}t\right|^2 \quad (1)$$

where * represents the complex conjugate operation, s is the scaling parameter which controls the width of the wavelet, while τ controls its location in the time domain. The WPS (Eq. (1)) can be interpreted as the local variance of the analysed signal.

This quantity can be averaged over time (τ) to obtain what is called the global WPS,

$$\int_{-\infty}^{+\infty}|W_{x;\psi}(\tau,s)|^2d\tau \quad (2)$$

The peaks in the global WPS indicate the major periods present in the signal. The periodicity is normally the effect of external, seasonal, forcing onto the considered signal, and therefore it should be conveniently removed. After being recognized by means of the CWT, the periodic components can be reconstructed and used for filtering purposes. The major cycles have a typical main frequency as identified by the maximum values in the global WPS curve, but actually, they occupy a frequency band of variable width. For a more complete reconstruction of the periodic signal, we use the whole frequency band, modulating the single frequencies of the band according to their wavelet power over the observation period. The bands are identified computing the second derivative of the global power spectrum and selecting the frequencies corresponding to the maximum values (i.e. peaks of the acceleration) as the band limits. We verified that this method is able to well isolate the WPS peaks without including unwanted low-power frequencies, or, on the other hand, excluding some high-power frequencies.

For this research we also aim to investigate and quantify the dependencies between two non-stationary time series (i.e. CO_2 and climatic variables). The cross-wavelet analysis is able to provide useful information such as the similarity (coherence) between the pair of wavelet power spectra and the series' synchronicity, namely the phase difference at a given periods (Grinsted et al., 2004). The cross-wavelet power is defined as:

$$(\mathrm{XPW})_{x,y}(\tau,s)=|W_{x;\psi}(\tau,s)W^*_{x;\psi}(\tau,s)| \quad (3)$$

where $W_{x;\psi}(\tau,s)$ and $W^*_{x;\psi}(\tau,s)$ are CWT (Eq. (1)) of the functions $x(t)$, $y(t)\in R$ which product is the cross-wavelet transformation. Conversely from the WPS (Eq. (1)) which can be interpreted as the local variance of the time series, the cross-wavelet power spectrum (Eq. (3)) represents the local covariance between the two compared time series for each time and frequency. It is a measure of the similarity of power between the two series. The global cross-wavelet power at the scale s, is defined as the time-average of (Eq. (3)), and the peaks indicate the shared period between the two series.

The phase difference between the two series ($\varphi_x(\tau,s)-\varphi_y(\tau,s)$) provides information about the synchronicity of the two series. A phase-difference less than $|\pi/2|$ indicates that the time series move together at a specific time-frequency (in-phase), an absolute value greater than $|\pi/2|$ indicates that the two series move out of phase.

In this paper, the wavelet transform and the global power spectrum are computed with the *WaveletComp* package Roesch et al. (2014) in the *R* statistical software R Development Core Team (2005).

Obviously, the longer the series, the more reliable are the results of the CWT. However, even with relatively short time series, this methodology allows the detection of the presence of persistence periodicity.

2.2. Data collection and characterization

At Mt. Etna Volcano the CO_2 monitoring is performed by a network (ETNAGAS network) which is operational since the early 2000s. In 2011 the network reached its present-day configuration which includes 14 sites distributed across the volcanic edifice. The hardware of the stations of ETNAGAS network is based on the measurement method proposed by Gurrieri and Valenza (1988) and it consists of a probe, which permits the gas to stations of be pumped from the ground by mixing it with air. The dilution ratio depends mainly on three factors: (a) the geometry of the probe; (b) the depth of insertion of the probe into the ground; and (c) the flow rate of the gases, mixed inside the probe. The CO_2 concentration value obtained with this method is proportional to the CO_2 flux released from the ground. The method was successively calibrated in the laboratory using a soil sample, which was exposed to CO_2 flux under controlled conditions. The equation, originally proposed by the authors, was subsequently modified by Camarda et al. (2006) to introduce soil permeability, a parameter which influences the measurement and, therefore, the calculated CO_2 flux.

Table 1
List of the soil CO_2 monitoring sites: geographical locations and number of hourly samples. IQR: Interquartile range of the CO_2 flux time series (values in kg m^2 d^{-1}).

Name	Lat.(°N)	Long.(°E)	Elev.(m)	CO_2	Air temp.	Atm. press.	Rel. hum.	IQR_{CO_2}
Agro	37.5336	14.8989	122	62998	64980	64980	64980	0.14
Albano1	37.7253	14.9422	1724	63016	6330	-	-	0.21
Brunek	37.8081	15.0742	1418	54798	54933	-	-	0.92
Fondachello	37.7706	15.2167	11	64850	65257	65257	-	0.62
Maletto	37.7936	14.8997	1192	65876	-	-	-	0.17
msm1	37.8258	14.9836	1535	67364	67364	67364	-	0.13
p78	37.6953	15.1433	324	64916	65110	-	65077	1.84
Parcoetna	37.6306	15.0231	836	66492	67027	-	40146	0.18
Passop	37.8669	15.0456	704	64181	65178	-	-	0.2
Roccacampana2	37.8003	15.1369	736	61841	-	61845	-	0.04
sml1	37.6569	14.9208	878	58743	-	44825	-	0.05
sml2	37.6636	14.9050	855	63163	64162	64162	64162	0.02
sv1	37.6967	15.1353	378	68365	-	67929	-	2.2
3c	37.6086	15.0822	518	63065	63110	63110	63032	0.14

The geometric configuration of the monitoring stations is the same for all the sites: in particular the insertion depth of the probe is fixed (i.e. 0.45 m). Measurements are taken hourly. In many sites, co-located sensors record air temperature, atmospheric pressure, and relative humidity at the same sampling rate. Rainfall data were also available at some sites, but not taken into account in the data analysis because the influence of the precipitation on the CO_2 flux is considered negligible at Mt. Etna (Liuzzo et al., 2013). Wind speed and direction are other variables which can potentially influence the CO_2 output, but unfortunately such information is not available for ETNAGAS network. The analysed time series of this study cover more than eight years: they range from January 2011 to March 2019. Table 1 lists the monitoring sites in terms of geographical coordinates, elevation, and number of hourly samples. The interquartile range (IQR), as a measure of the dispersion of the CO_2 time series is also provided.

In order to highlight the general statistical characteristics of the CO_2 time series, we calculated the kernel density plots (Fig. 1). They show different distributions: small-scale relative maxima are overlapped to a general uni-modal, asymmetric distribution. Values range from 0 to ~1 kg m^2 d^{-1} for 10 out of 14 sites, for two sites ("brunek" and "fondachello") they range from 0 to ~3 kg m^2 d^{-1}, while they are almost

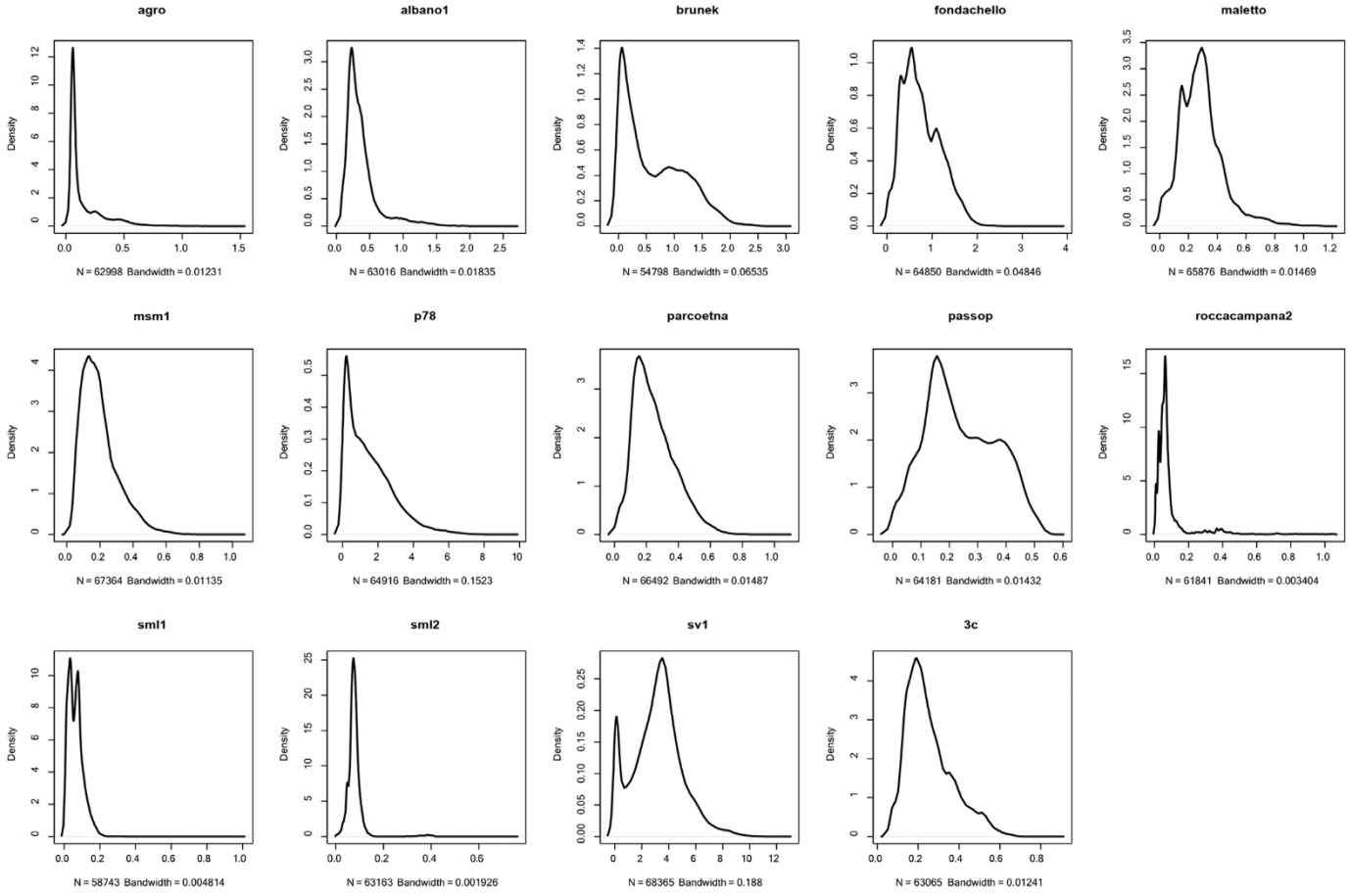

Fig. 1. Kernel density plots of soil CO_2 for the 14 sites (values in kg m^2 d^{-1}); bandwidths are selected according to Scott's rule (Scott, 1992).

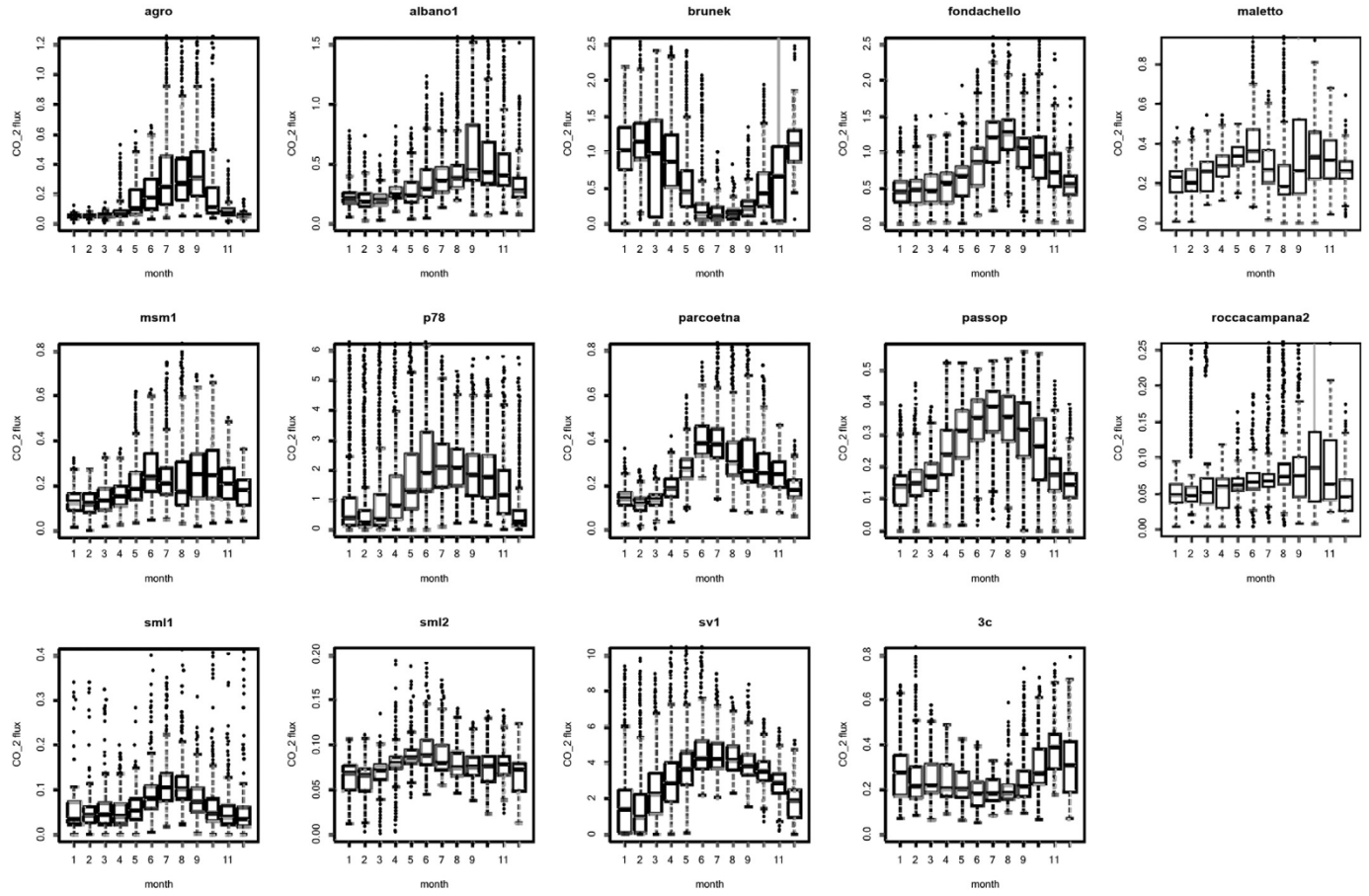

Fig. 2. Box plots of hourly soil CO_2 flux values classified by month (values in kg m^2 d^{-1}).

one order of magnitude greater (0 to ~11 kg m^2 d^{-1}) for the sites "p78", and "sv1". The kernel density plots suggest the occurrence of different sub-population in the CO_2 flux at several monitoring sites, each one resulting from different processes. The occurrence of several sub-populations in the soil CO_2 flux is already documented at Mt. Etna volcano (Giammanco et al., 2010; Liuzzo et al., 2013) but examining the details is out of the scope of this work. However, this is the reason why raw flux data should be somehow filtered. As already stressed, it is essential to remove the climatic-environmental effects. A first evidence of seasonal variations of the flux emerges classifying the data by month (Fig. 2). In most of the cases the largest CO_2 outputs occur in the hot, dry season (June (6) to September (9)), in some sites this behaviour is less marked, while in some others (e.g. "brunek" and "3c") the behaviour is even opposite.

Data have been pre-processed: first, time series of daily soil CO_2 fluxes (and also the available variables) were calculated considering the median value from the hourly samples; second, missing data have been replaced by means of a cubic spline interpolation, but only for interruption shorter than 7 days. This is an effective way to handle missing data in a time series when the missing values span over few

Table 2
List of the periodic, continuous components detected with the wavelet analysis (values are in days). $T1_{CO_2}$ and $T2_{CO_2}$ are the main and the subordinate periods for CO_2 time series respectively, where the corresponding band limits are limits $T1_{CO_2}$ and limits $T2_{CO_2}$. The main components of the cross-wavelet analysis are also reported when available: *T*: air temperature; *P*: atmospheric pressure; *H*: relative humidity; n.a.: not applicable.

Site	days	$T1_{CO_2}$	$T2_{CO_2}$	Limits $T1_{CO_2}$	Limits $T2_{CO_2}$	T_{CO_2-T}	T_{CO_2-P}	T_{CO_2-H}
Agro	902	340	115	247:461	97:137	350	340	350
Albano1	1047	375	165	274:495	111:201	350	-	-
Fondachello	912	305	125	201:461	87:163	350	320	-
Maletto	964	210	130	158:256	104:158	-	-	-
msm1	1702	360	-	274:461	-	350	350	-
p78	2058	375	-	284:446	-	370	-	365
Parcoetna	1082	360	-	256:494	-	360	-	-
Passop	1150	360	-	265:494	-	360	-	-
Roccacampana2	1145	375	-	284:512	-	-	340	-
sml1	873	350	180	247:461	137:247	-	n.a.	-
sml2	821	165	295	115:215	215:375	305	305	300
sv1	1699	360	-	274:446	-	-	365	-
3c	657	135	70	111-158	52:84	350	340	340

time points (Lepot et al., 2017). If, from one hand, the averaged daily time series remove the high-frequency noise, from the other hand they do not allow to identify the existence of any diurnal or semidiurnal cycles. The wavelet analysis has been applied to the longest uninterrupted portions of signal at each site which varies from 657 days at "3c" site to 2068 at "p78" (Table 1).

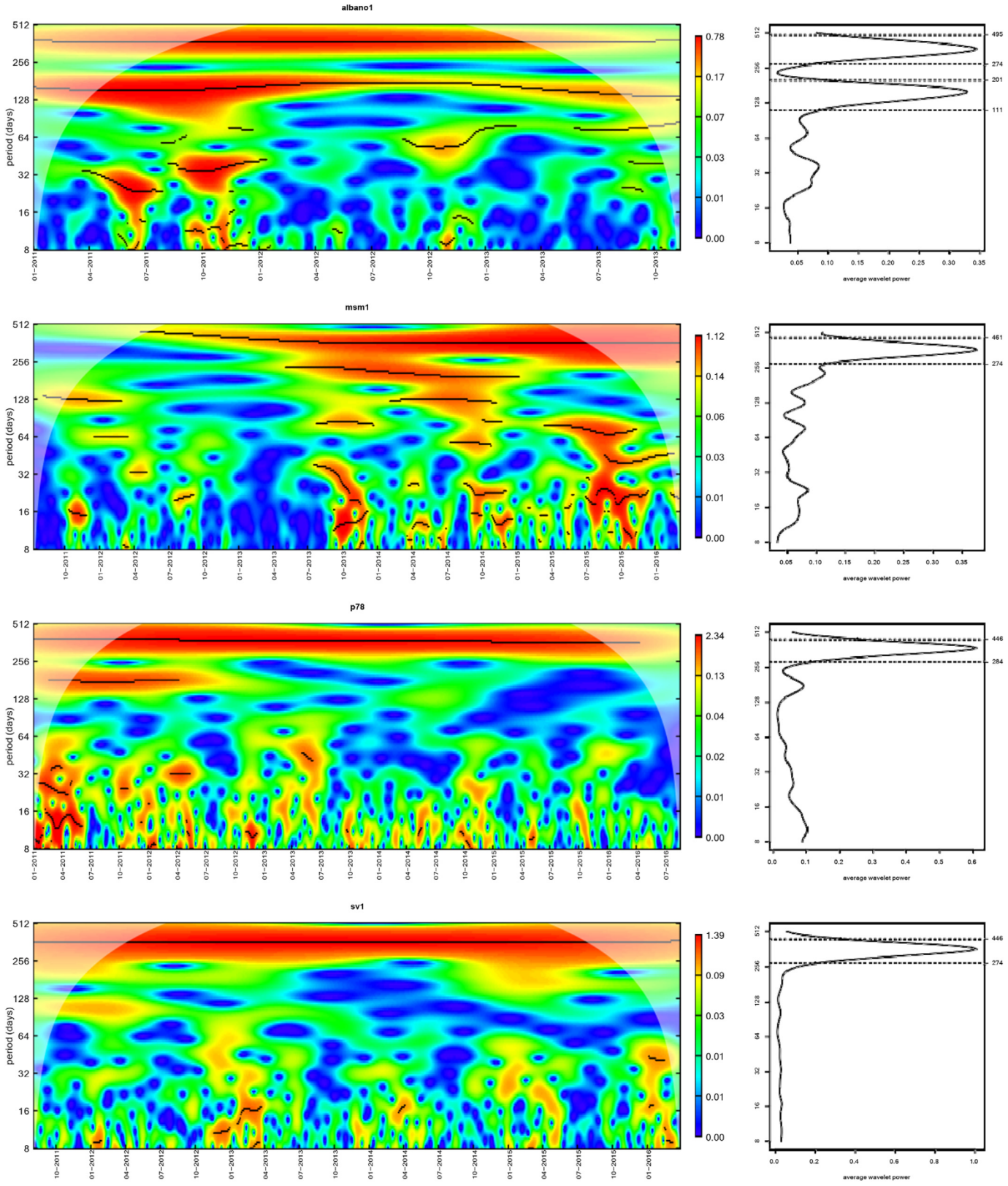

Fig. 3. Wavelet power spectrum of daily soil CO_2 series in time-frequency domain with the CWT method for a selection of 4 sites: "albano1", "msm1", "p78", and "sv1" (left column). The black contour indicates the significant period with 90% confidence level. The shaded regions indicate the possible influence of edge effects. The corresponding power spectrum density averaged over time is in the right column; the limits of the bands are reported (dashed lines).

When performing the coherency between pairs of series, the period with commonly available data could be shorted than reported in the Table 1.

3. Results

The results of the wavelet power spectrum analysis and of the cross-wavelet analysis are listed in Table 2. Because of the frequent interruptions, it has not been possible to perform the analysis at "brunek" site. The values in the axis of the period are discrete, therefore the maximum values for the periods are rounded to the closest value in a 5-days stepped scale. The limits of the bands for the CO_2 periods are also reported. Only the periods with a level of significance >0.1, and continuous over the analysed period, are reported in the Table 2. The significance tests of the null hypothesis of no (or no joint in case of cross-wavelet analysis) periodicity tested against simulated time series. The continuity prerequisite derives from the assumption of correlation between the observed periods of CO_2 time series with the main periods of the climatic variables, which are persistent. These are the components to be filtered first (Viveiros et al., 2014). Of course, the wavelet analysis is capable to highlight non-stationary phenomena, but those usually represent the targets to be highlighted in the residuals.

All the sites, except "maletto", "sml2", and "3c", show a main peak of the wavelet power roughly corresponding to the annual cycle (i.e. 340–370 days). Such a yearly cycle was largely expected because of previous works regarding signals from the same network and because of

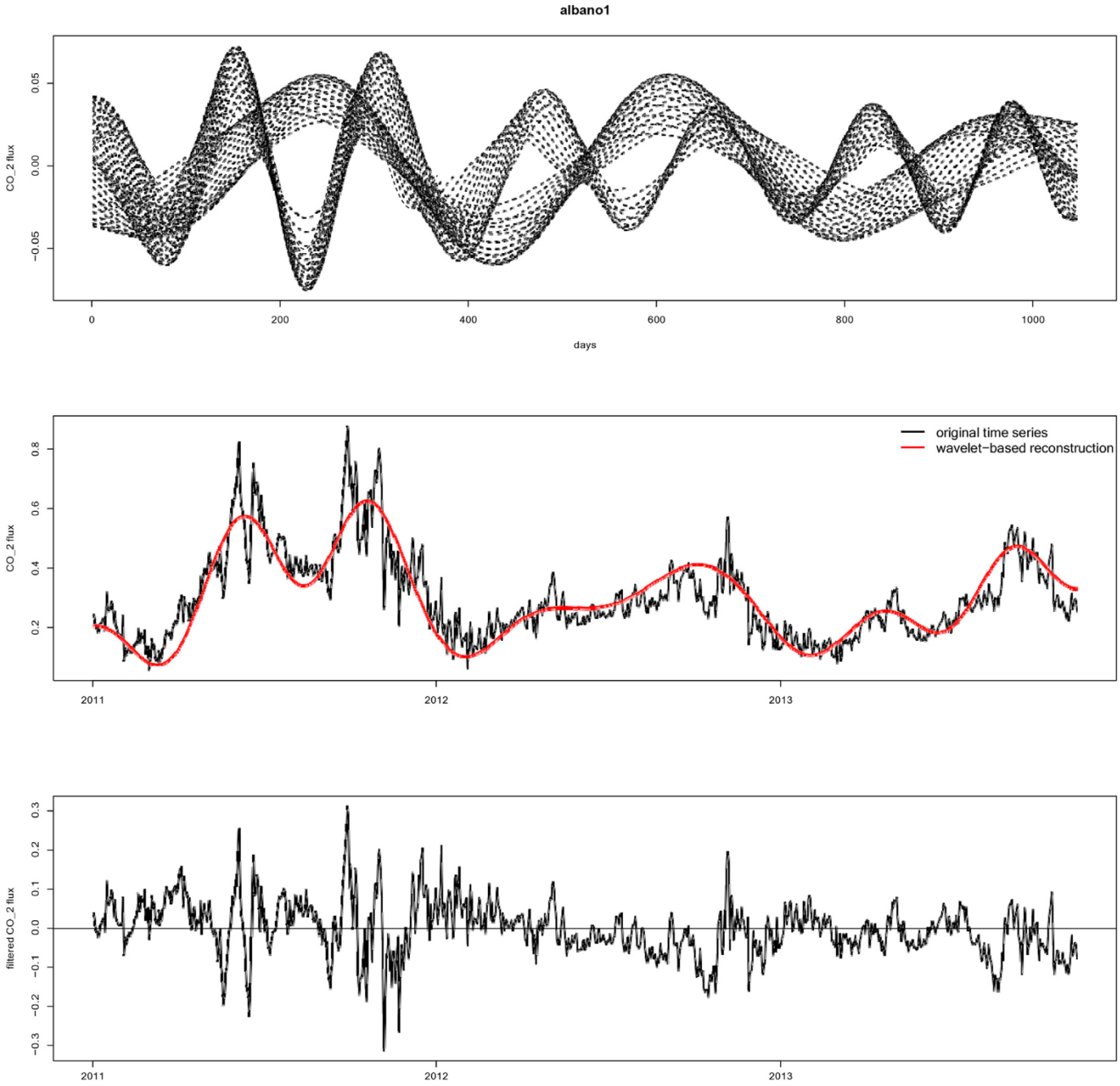

Fig. 4. Example of signal reconstruction and filtering for the site "albano1", characterized by two main periods (c.f. Table 2). Reconstructed waves within the two recognized bands (top) are used to reproduce the periodic component which is used to filter the original signal (centre) and calculate the residual flux values after the filtering (bottom). CO_2 flux is in kg m^2 d^{-1}.

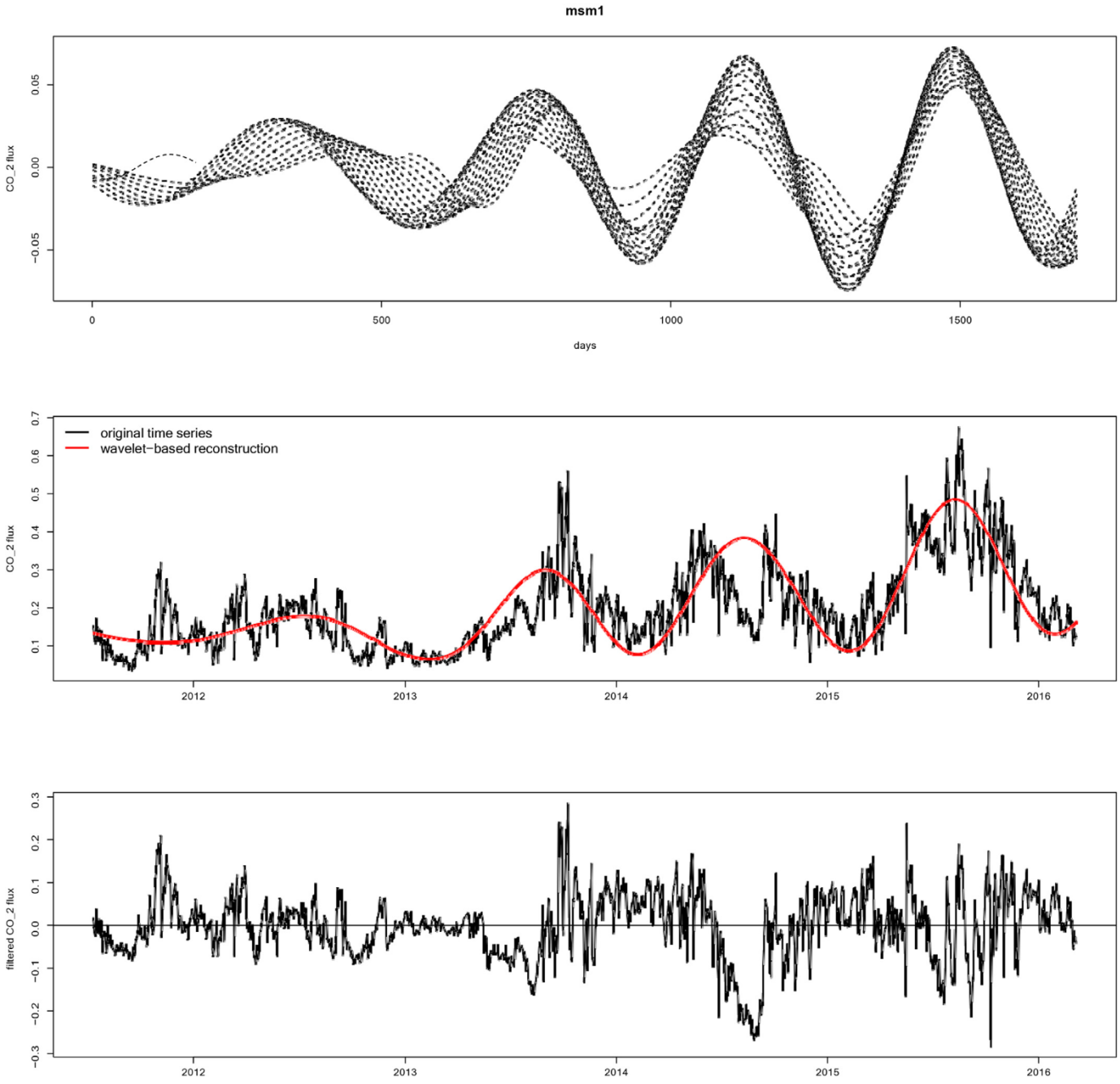

Fig. 5. Example of signal reconstruction and filtering for the site "msm1", characterized by a single main periods (c.f. Table 2). Reconstructed waves within the recognized band (top) are used to reproduce the periodic component which is used to filter the original signal (centre) and calculate the residual flux values after the filtering (bottom). CO_2 flux is in kg m^2 d^{-1}.

the vast literature about soil gas emission (Liuzzo et al., 2013; Viveiros et al., 2014; Oliveira et al., 2018; Gurrieri et al., 2021; Lewicki, 2021). Fig. 3 shows the wavelet power spectrum for a selection of four among the sites. When it is present, the annual cycle is continuous over the whole period. Sub-ordinate periods of shorter duration occur at some sites (Table 2). These may vary from ~70 to ~300 days and they are not always continuous over the whole observation period. Even shorter periodicities (less than <~100 days) with limited durations (usually some months) emerge at some sites. Such pulsations have been put in relationship with the eruptive processes (intrusions and eruptions) (Gurrieri et al., 2008; Berberich et al., 2019) and may vary according to the site's location with respect the volcanic edifice.

The periodic signals, or rather every single component within the frequency bands of Table 2, can be reconstructed and therefore filtered. Figs. 4 and 5 show two examples of filtering in sites where a double ("albano1") and a single peak ("msm1") have been highlighted by the power spectrum analysis. The waves corresponding to the single discrete frequency in the band have been modulated according to their power spectrum (Fig. 3), then combined together. The resulting signals (red lines in Figs. 4 and 5) can be used to filter the time series from the periodic components. At glance, both positive and negative anomalies emerge in the residual flux after filtering the signals, which can be therefore volcanologically interpreted excluding any seasonal effect. A detailed analysis of these short-term features could provide insights about the dynamics of magma recharge or about the eruptions at Mt. Etna. However, this paper focuses on the methodological approach, and the systematic analysis of the anomalies in relation to the volcanic activity is out of the scope of the paper.

The cross-wavelet analysis highlights common periods between the CO_2 signals and each of the climatic variables, when available; results are reported in Table 2 and shown in Figs. 6 and 7 for the sites "agro" and "3c", respectively. In these sites, we have the full availability of all the data (CO_2 and climatic ones). Results indicate that the time series are highly correlated and the joint annual cycle is continuous over the analysed period and for all the variables, even though it is characterized by a different power. In a narrow band (20-days) corresponding to the maximum value of the cross-wavelet power we computed the phases of CO_2 series and of the climatic series. The resulting phase differences are the black dashed lines in Figs. 6 and 7; they are constant, or almost constant over time. The couple of series is in phase when the phase difference is almost null; they are out of phase when the phase difference approaches the value $\pm\pi$. Comparing the results at the different monitoring sites, the behaviour of the climatic variables appear to be consistent through time but site-specific. Summing up, the annual cycle of CO_2 flux is affected by the climatic variations over a year (Liuzzo et al., 2013; Gurrieri et al., 2021), even though their synchronicity may vary.

Given the information about the phases and phase difference of the joint annual period, we analytically calculated the harmonics of the

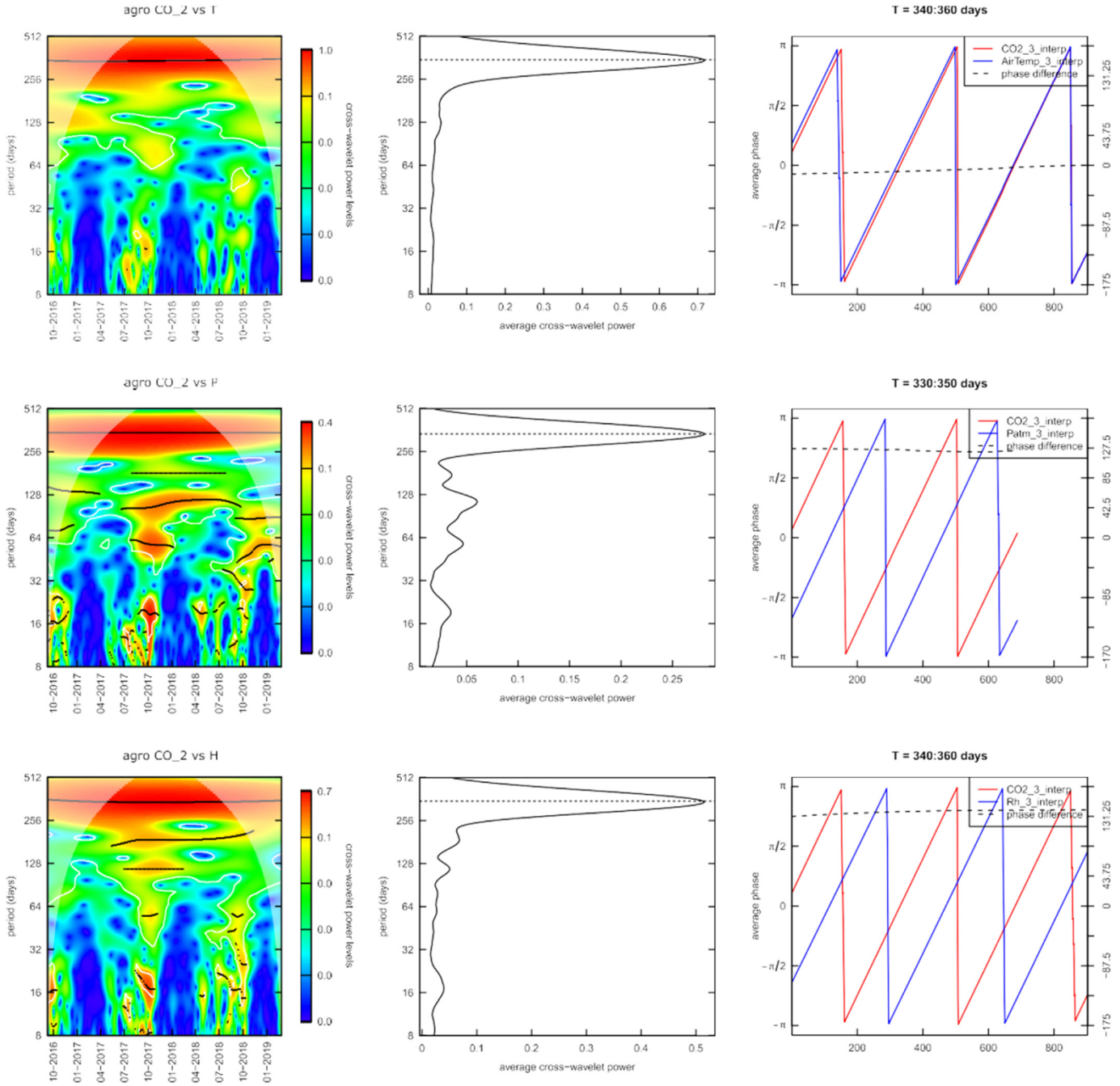

Fig. 6. Left column: cross-wavelet power spectrum between CO_2 and air temperature (T), atmospheric pressure (P), and relative humidity (H) for the site "agro". Central column: cross-wavelet power spectrum averaged over time; reference lines are at 350, 340, and 350 days respectively. Right column: phases and phase differences between CO_2 and climatic time series calculated at the peak period.

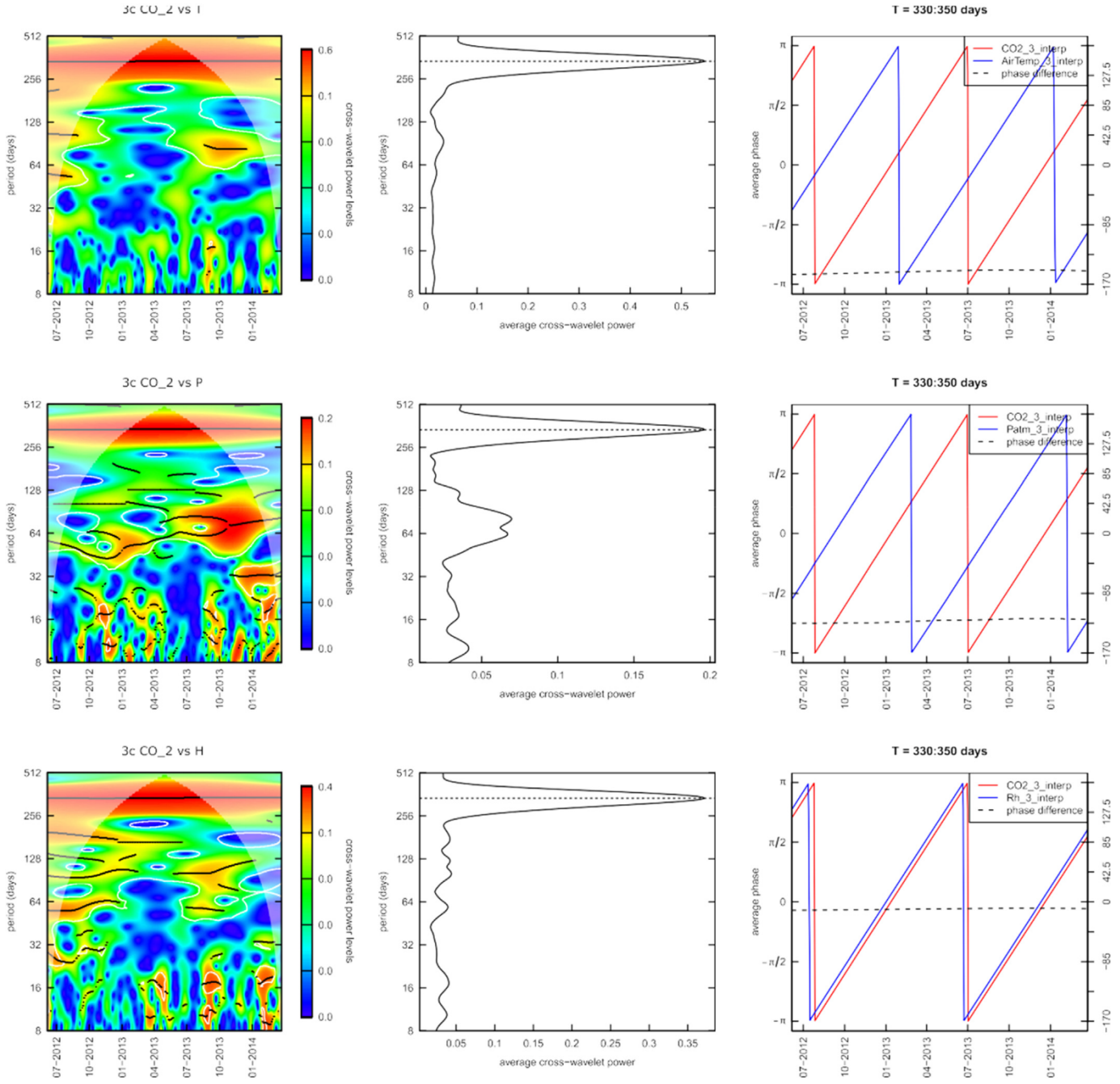

Fig. 7. Left column: cross-wavelet power spectrum between CO_2 and air temperature (T), atmospheric pressure (P), and relative humidity (H) for the site "3c". Central column: cross-wavelet power spectrum averaged over time;; reference lines are at 350, 340, and 340 days respectively. Right column: phases and phase differences between CO_2 and climatic time series calculated at the peak period.

climatic variables, again for the sites "agro" and "3c" (Fig. 8 and 9). To account for their relative influence, the amplitudes of these harmonics are proportional to the maximum values of the average cross-wavelet power in the same band (Table 3). This value is a measure of the similarity of power between two series and it is independent from the length of the series. For "agro" these weights are 0.72, 0.28, and 0.51 for air temperature, atmospheric pressure, and relative humidity respectively; for "3c" they are 0.55, 0.20, and 0.37 respectively. Interestingly, the ratios between the weights of the climatic variables are almost constant. The sum of the harmonics, normalized in the interval 0–1, is then compared to the flux of CO_2, showing a clear correspondence of the yearly minimum and maximum values. The Pearsons' correlation coefficients are 0.79 and 0.71 for "agro" and "3c" respectively and indicate a very good level of linear correlation. The calculated combined effect of the climatic components has been extended for three cycles also to other portions of the CO_2 signal (before and after respectively). Finally, the "climatic effect" has been converted into flux unit (kg m^2 d^{-1}) fitting the harmonic into the range of values (difference between the maximum and the minimum flux over the considered period) of CO_2 flux (Figs. 8 and 9).

4. Discussion and conclusions

We exploited data coming from a CO_2 flux monitoring network to perform a time-frequency analysis based on the continuous wavelet transformation. The CO_2 flux in volcanic areas can be used as a proxy

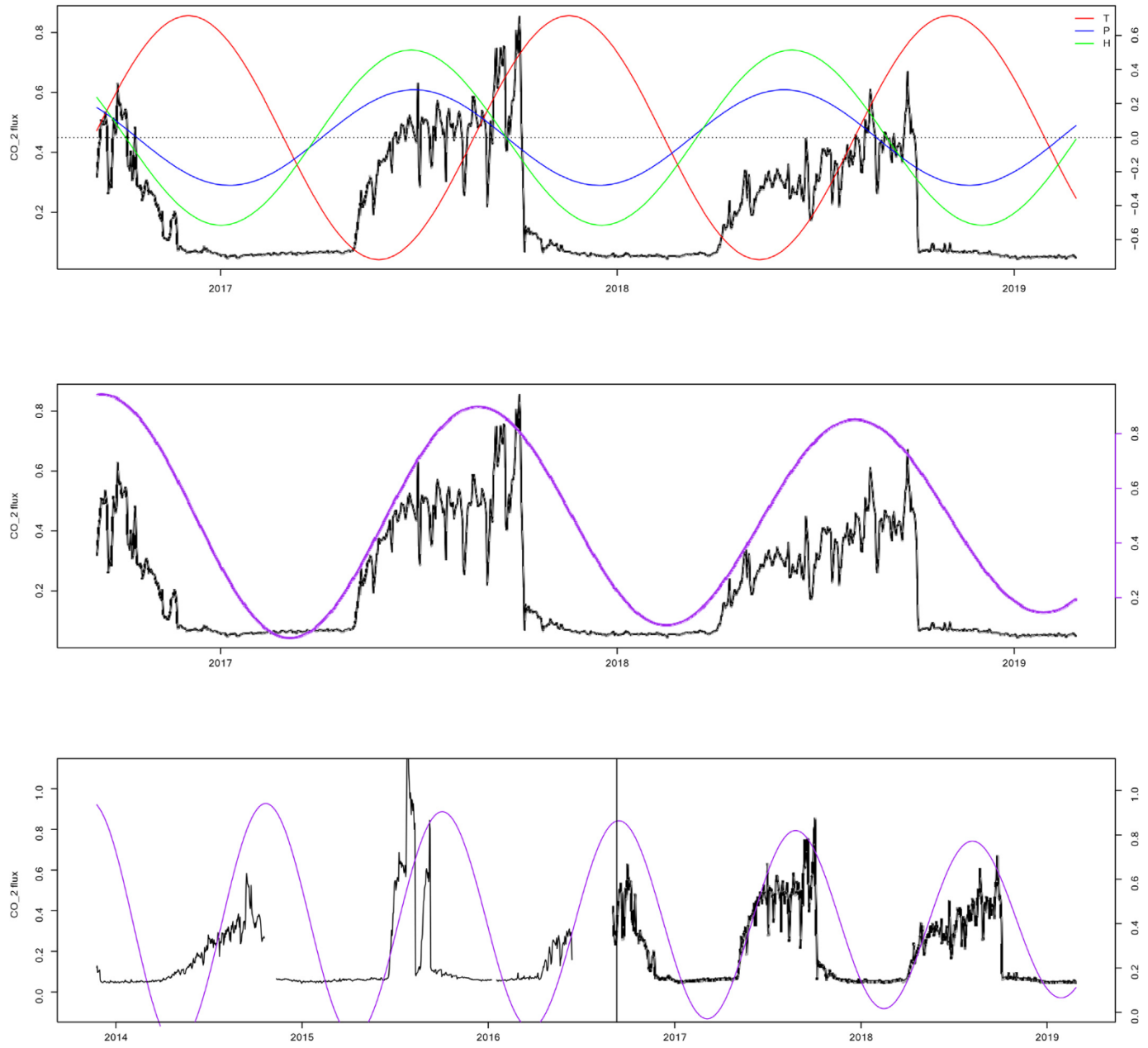

Fig. 8. Top row: CO_2 flux (in kg m^2 d^{-1}) and the analytical signal of air temperature (T), atmospheric pressure (P), and relative humidity (H) for the site "agro"; the curves have been calculated from the periods, phase differences, and power obtained by the cross-wavelet analysis (Tables 2 and 3). Central row: comparison between the CO_2 flux and the combined effect (climatic component) of T, P, and H (sum). Bottom row: climatic component converted into flux unit (in kg m^2 d^{-1}) and extended before the period of its calculation; the vertical line represents the limit.

for the volcanic activity, and therefore its study reveals of great importance. However, before looking for any volcano-related anomaly, the time-frequency characterization of the flux is desirable, and the signal should be conveniently filtered. For this purpose, the decadal CO_2 time series from Mt. Etna, even with some interruptions, enable a robust analysis. Tests on simulated data demonstrate that the wavelet technique is able to point out a given period even when the time series is shorter than twice the same period (Siino et al., 2019). Therefore, the occurrence of interruptions in the CO_2 time series which prevent performing the time-frequency analysis over a longer period, do not represent a limitation, rather results about the main cycles can be extended in time beyond the time interval they have been calculated. Because of these considerations, we are very confident about the reliability of the results.

Results highlight the occurrence of annual variations of the CO_2 flux at most all of the sites. Secondary, shorter, periods may occur at some sites. All these periods coincide with global phenomena with similar frequency and therefore they can be interpreted as dependent on the atmospheric cycles (Viveiros et al., 2014). We propose a wavelet-based filtering technique for these periodic components of the signal, which enable to enhance the anomalies related to the volcanic processes. Moreover, the so filtered time series can be easily compared or even combined together, to get insights on the dynamics of CO_2 flux at the scale of the whole volcano (Liuzzo et al., 2013; Gurrieri et al., 2021).

Correlation between CO_2 and environmental variables has been reported in various volcanic regions (Granieri et al., 2003; Rinaldi et al., 2012; Lewicki and Hilley, 2014; Viveiros et al., 2014; Morita et al., 2019; Lewicki, 2021) and also at Mt. Etna (Liuzzo et al., 2013).

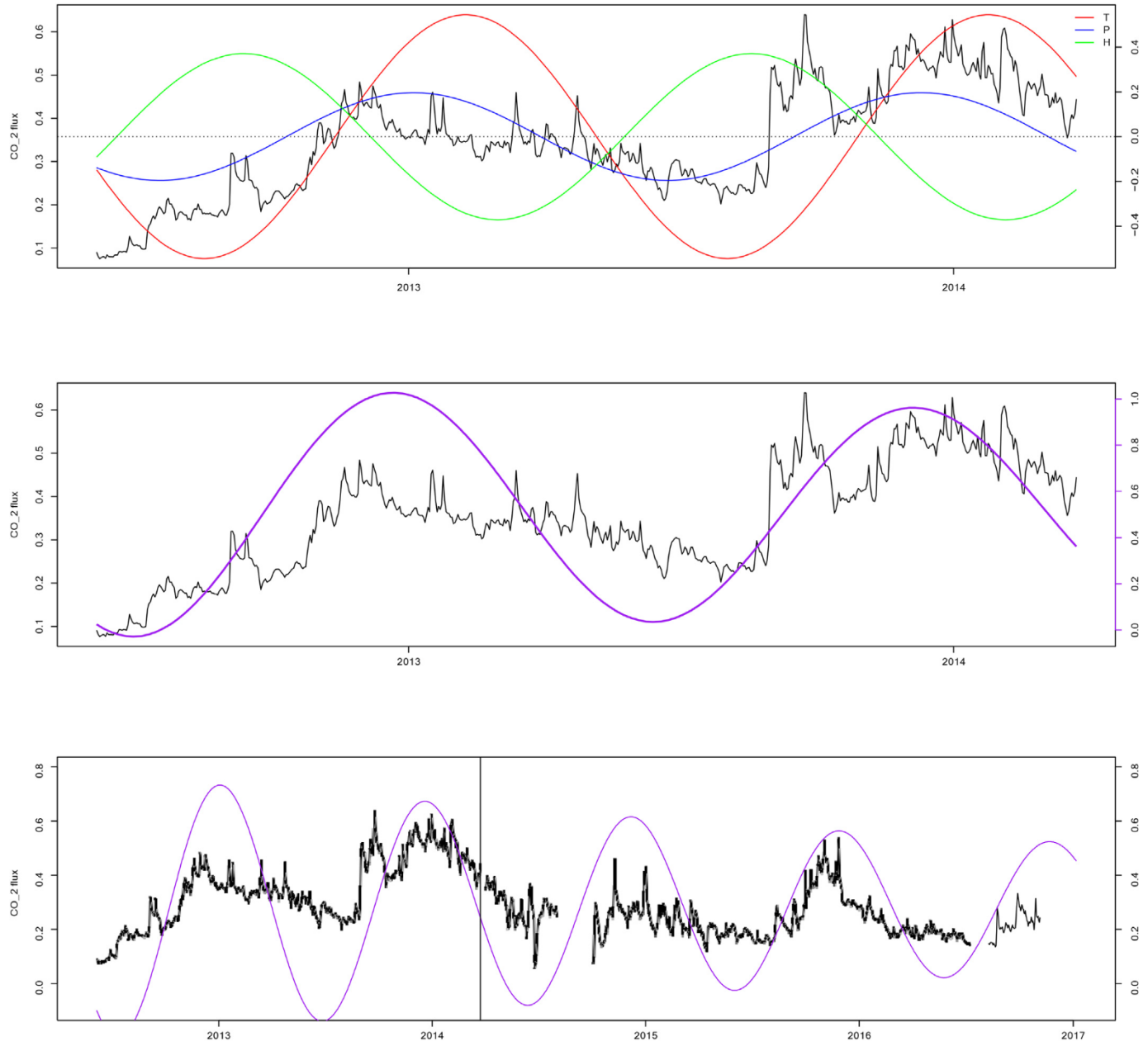

Fig. 9. Top row: CO_2 flux (in kg m^2 d^{-1}) and the analytical signal of air temperature (T), atmospheric pressure (P), and relative humidity (H) for the site "3c"; the curves have been calculated from the periods, phase differences, and power obtained by the cross-wavelet analysis (Tables 2 and 3). Central row: Comparison between the CO_2 flux and the combined effect (climatic component) of T, P, and H (sum). Bottom row: climatic component converted into flux unit (in kg m^2 d^{-1}) and extended after the period of its calculation; the vertical line represents the limit.

Therefore, the coherency between the CO_2 signals and each of the climatic variables is explored with the cross-wavelet analysis. Moreover, the availability of full meteorological information at some locations allowed us to model their effects on the CO_2 flux from the analytical combination of the climatic variables. In this case study, the modulation of the meteorological variables on the CO_2 flux is suggested by: (i) the occurrence of annual joint cycles both in the CO_2 and climatic time series and (ii) the fit between the analytically solved "climatic effect" and the CO_2 flux time series. Therefore the observed periodic variations are not ascribable to changes in the gas source properties.

Table 3
Maximum values of the average cross-wavelet power for the sites with complete information of the climatic variables and average phase difference values (in *rad*) at the corresponding period (c.f. Table 2).

	Air temperature		Atm. pressure		Rel. humidity	
Site	Power	Phase diff.	Power	Phase diff.	Power	Phase diff.
Agro	0.717	−0.13	0.281	2.29	0.515	2.48
sml2	0.216	−0.83	0.086	0.12	0.162	0.95
3c	0.545	−2.80	0.196	−2.29	0.371	−0.19

The control mechanisms of the climatic variables onto the soil CO_2 flux is not fully understood (Viveiros et al., 2014; Lewicki, 2021). Numerical models proposed by Rinaldi et al. (2012) and Viveiros et al. (2014) suggest both direct effects of these parameters on the mobility of CO_2 through changes in its density and viscosity, as well as indirect effects on the flow dynamics of the shallower degassing system through changes in the gradient. However, it is not easy to isolate the effects of a single variables (i.e. air temperature, atmospheric pressure,

relative humidity, wind speed, rainfall, etc), as they normally act simultaneously. The air temperature is considered as responsible of the most of the seasonal variation because of its control on CO_2 mobility (Rinaldi et al., 2012), while the atmospheric pressure exerts only a secondary influence (Lewicki, 2021). Also in the Etna case study, the greatest influence would be in charge on the air temperature as indicated by the cross-wavelet power (Table 3), followed by the relative humidity and, finally, the atmospheric pressure.

Results suggest that the meteorological variables control the annual variations of CO_2; the exact mechanism cannot directly seized, however the results indicate that the way they combine (i.e. synchronicity or phase difference) would be controlled by local factors. A limitation to this case study is represented by the unavailability of the climatic data for all the sites, which prevents examining in depth their relationship with the variability of the CO_2 emissions. Nevertheless, the results coming from the only three sites with complete information (Table 3), suggest that a controlling mechanism related to the local environmental parameters affects the soil CO_2 emissions. The phase difference between CO_2 and the three climatic variables is site-specific, but their relative influence, as suggested by the averaged cross-wavelet power, appears to be consistent between the various sites. In fact, in these three sites, the ratios between the maximum cross-wavelet power for the three pairs of climatic variables are constant (c.f. Table 3). This evidence suggests a general mechanism regulating the dynamics of the CO_2 flux, while the properties of the local system (i.e. exposure, elevation, local permeability at the site, etc.) may control only the phase shifts of the single climatic variable (Table 3). Such constant time shifts have been observed, even though in daily cycles, also by Rinaldi et al. (2012) and can be viewed as the transfer functions between a certain climatic variable and the CO_2 flux due to the unique set of characteristics at the monitoring site (Lewicki, 2021).

The signal obtained from the climatic variables can be used as a baseline to predict the seasonal trend of the CO_2 output and, therefore, to evaluate anomalies in real-time. It also may be useful to reconstruct missing portions in the data in case of temporary malfunctioning of the CO_2 sensors.

Finally, the proposed methodology can be successfully applied in any other sites and also for other types of soil gases which emissions are usually strongly controlled by the climatic variables.

Data availability

The raw time series of soil CO_2 data are available upon request to Marco Liuzzo (marco.liuzzo@ingv.it).

Declaration of Competing Interest

The authors declare that they have no known competing financial interests or personal relationships that could have appeared to influence the work reported in this paper.

Appendix A. Supplementary data

Supplementary data to this article can be found online at https://doi.org/10.1016/j.jvolgeores.2021.107421.

References

Berberich, G.M., Berberich, M.B., Ellison, A.M., Wöhler, C., 2019. First identification of periodic degassing rhythms in three mineral springs of the east Eifel volcanic field (Eevf, Germany). Geosciences 9 (4), 189.

Boichu, M., Oppenheimer, C., Tsanev, V., Kyle, P.R., 2010. High temporal resolution SO_2 flux measurements at Erebus volcano, Antarctica. J. Volcanol. Geotherm. Res. 190 (3-4), 325–336.

Camarda, M., Gurrieri, S., Valenza, M., 2006. CO_2 flux measurements in volcanic areas using the dynamic concentration method: iznfluence of soil permeability. J. Geophysci. Res.: Solid Earth 111 (B5.).

Cannata, A., Coauthors, 2015. Pressurization and depressurization phases inside the plumbing system of mount Etna volcano: evidence from a multiparametric approach. J. Geophysci. Res.: Solid Earth 120 (9), 5965–5982.

Conraria, L.A., Soares, M.J., 2011. The Continuous Wavelet Transform: A Primer. NIPE Working Paper, 16. pp. 1–43.

D'Alessandro, A., Scudero, S., Siino, M., Alessandro, G., Mineo, R., 2020. Long-term monitoring and characterization of soil radon emission in a seismically active area. Geochem. Geophys. Geosyst. 21 (7), e2020GC009061. https://doi.org/10.1029/2020GC009061.

Daubechies, I., 1992. Ten Lectures on Waveletsvol. 61. Siam.

Giammanco, S., Bellotti, F., Groppelli, G., Pinton, A., 2010. Statistical analysis reveals spatial and temporal anomalies of soil CO_2 efflux on mount Etna volcano (Italy). J. Volcanol. Geotherm. Res. 194 (1-3), 1–14.

Granieri, D., Avino, R., Chiodini, G., 2010. Carbon dioxide diffuse emission from the soil: ten years of observations at vesuvio and campi flegrei (pozzuoli), and linkages with volcanic activity. Bull. Volcanol. 72 (1), 103–118.

Granieri, D., Chiodini, G., Marzocchi, W., Avino, R., 2003. Continuous monitoring of CO_2 soil diffuse degassing at phlegraean fields (Italy): influence of environmental and volcanic parameters. Earth Planet. Sci. Lett. 212 (1-2), 167–179.

Grinsted, A., Moore, J.C., Jevrejeva, S., 2004. Application of the cross wavelet transform and wavelet coherence to geophysical time series. Nonlinear Process. Geophys. 11 (5/6), 561–566.

Gurrieri, S., Liuzzo, M., Giudice, G., 2008. Continuous monitoring of soil CO_2 flux on Mt. Etna: the 2004–2005 eruption and the role of regional tectonics and volcano tectonics. J. Geophysci. Res.: Solid Earth 113, B09206. https://doi.org/10.1029/2007JB005003.

Gurrieri, S., Liuzzo, M., Giuffrida, G., Boudoire, G., 2021. The first observations of CO_2 and CO_2/SO_2 degassing variations recorded at Mt. Etna during the 2018 eruptions followed by three strong earthquakes. Ital. J. Geosci. 140 (1), 95–106.

Gurrieri, S., Valenza, M., 1988. Gas transport in natural porous mediums: a method for measuring CO_2 flows from the ground in volcanic and geothermal areas. Rend. Soc. Ital. Mineral. Petrol 43, 1151–1158.

Ilanko, T., Oppenheimer, C., Burgisser, A., Kyle, P., 2015. Cyclic degassing of Erebus volcano, Antarctica. Bull. Volcanol. 77 (6), 1–15.

Lepot, M., Aubin, J.-B., Clemens, F.H., 2017. Interpolation in time series: an introductive overview of existing methods, their performance criteria and uncertainty assessment. Water 9 (10), 796.

Lewicki, J.L., 2021. Long-term year-round observations of magmatic CO_2 emissions on mammoth mountain, California, USA. J. Volcanol. Geotherm. Res. 418, 107347.

Lewicki, J.L., Hilley, G.E., 2014. Multi-scale observations of the variability of magmatic CO_2 emissions, mammoth mountain, CA, USA. J. Volcanol. Geotherm. Res. 284, 1–15.

Lewicki, J.L., Kelly, P.J., Bergfeld, D., Vaughan, R.G., Lowenstern, J.B., 2017. Monitoring gas and heat emissions at norris geyser basin, yellowstone national park, USA based on a combined eddy covariance and multi-gas approach. J. Volcanol. Geotherm. Res. 347, 312–326.

Liuzzo, M., Gurrieri, S., Giudice, G., Giuffrida, G., 2013. Ten years of soil CO_2 continuous monitoring on Mt. Etna: exploring the relationship between processes of soil degassing and volcanic activity. Geochem. Geophys. Geosyst. 14 (8), 2886–2899.

Mallat, S., 1999. A wavelet tour of signal processing. Academic Press, Burlington, MA, USA https://doi.org/10.1016/B978-0-12-374370-1.50001-9.

Morita, M., Mori, T., Yokoo, A., Ohkura, T., Morita, Y., 2019. Continuous monitoring of soil CO_2 flux at aso volcano, Japan: the influence of environmental parameters on diffuse degassing. Earth Planets Space 71 (1), 1–16.

Oh, Y.-Y., Yun, S.-T., Yu, S., Kim, H.-J., Jun, S.-C., 2019. A novel wavelet-based approach to characterize dynamic environmental factors controlling short-term soil surface CO_2 flux: application to a controlled CO_2 release test site (Eit) in South Korea. Geoderma 337, 76–90.

Oliveira, S., Viveiros, F., Silva, C., Pacheco, J.E., 2018. Automatic filtering of soil CO_2 flux data; different statistical approaches applied to long time series. Front. Earth Sci. 6, 208.

Pering, T., Tamburello, G., McGonigle, A., Aiuppa, A., Cannata, A., Giudice, G., Patanè, D., 2014. High time resolution fluctuations in volcanic carbon dioxide degassing from mount Etna. J. Volcanol. Geothermal Res. 270, 115–121.

Pering, T.D., Ilanko, T., Liu, E.J., 2019. Periodicity in volcanic gas plumes: a review and analysis. Geosciences 9 (9), 394.

R Development Core Team, 2005. R: A Language and Environment for Statistical Computing. R Foundation for Statistical Computing, Vienna, Austria. http://www.R-project.org, ISBN 3-900051-07-0.

Rinaldi, A.P., Vandemeulebrouck, J., Todesco, M., Viveiros, F., 2012. Effects of atmospheric conditions on surface diffuse degassing. J. Geophysci. Res.: Solid Earth 117, B11201. https://doi.org/10.1029/2012JB009490.

Roesch, A., Schmidbauer, H., Roesch, M.A., 2014. Package 'waveletcomp'.

Scott, D., 1992. The curse of dimensionality and dimension reduction. Density Estimation: Theory, Practice and Visualizationpp. 195–217.

Sifuzzaman, M., Islam, M.R., Ali, M., 2009. Application of Wavelet Transform and its Advantages Compared to Fourier Transform.

Siino, M., Scudero, S., Cannelli, V., Piersanti, A., D'Alessandro, A., 2019. Multiple seasonality in soil radon time series. Sci. Rep. 9 (1), 1–13. https://doi.org/10.1038/s41598-019-44875-z.

Siino, M., Scudero, S., D'Alessandro, A., 2020. Stochastic Models for Radon Daily Time Series: Seasonality, Stationarity, and Long-Range Dependence Detection. Front. Earth Sci. 8, 575001. https://doi.org/10.3389/feart.2020.575001.

Tamburello, G., Aiuppa, A., McGonigle, A., Allard, P., Cannata, A., Giudice, G., Kantzas, E., Pering, T., 2013. Periodic volcanic degassing behavior: the mount Etna example. Geophys. Res. Lett. 40 (18), 4818–4822.

Viveiros, F., Ferreira, T., Silva, C., Gaspar, J.L., 2009. Meteorological factors controlling soil gases and indoor CO_2 concentration: a permanent risk in degassing areas. Sci. Total Environ. 407 (4), 1362–1372.

Viveiros, F., Ferreira, T., Silva, C., Vieira, J., Gaspar, J., Virgili, G., Amaral, P., 2015. Permanent monitoring of soil CO_2 degassing at furnas and fogo volcanoes (Sao Miguel Island, Azores). Geol. Soc. Lond. Mem. 44 (1), 271–288.

Viveiros, F., Vandemeulebrouck, J., Rinaldi, A.P., Ferreira, T., Silva, C., Cruz, J.V., 2014. Periodic behavior of soil CO_2 emissions in diffuse degassing areas of the Azores archipelago: application to seismovolcanic monitoring. J. Geophysci. Res.: Solid Earth 119 (10), 7578–7597.

Yan, R., Woith, H., Wang, R., Wang, G., 2017. Decadal radon cycles in a hot spring. Sci. Rep. 7 (1), 12120.